(submitted to Surf. Sci.)

The Pd(100)-($\sqrt{5} \times \sqrt{5}$)$R27^o$-O surface oxide revisited

M. Todorova[1], E. Lundgren[2], V. Blum[3], A. Mikkelsen[2], S. Gray[2],
J. Gustafson[2], M. Borg[2], J. Rogal[1], K. Reuter[1], J.N. Andersen[2], and M. Scheffler[1]
[1] *Fritz-Haber-Institut der Max-Planck-Gesellschaft, Faradayweg 4-6, D-14195 Berlin, Germany*
[2] *Department of Synchrotron Radiation Research, Institute of Physics, Lund University, Box 118, SE-221 00 Lund, Sweden and*
[3] *National Renewable Energy Laboratory, Golden, Colorado 80401, USA*

(Dated: February 2, 2008)

Combining high-resolution core-level spectroscopy (HRCLS), scanning tunneling microscopy (STM) and density-functional theory (DFT) calculations we reanalyze the Pd(100)-($\sqrt{5} \times \sqrt{5}$)$R27^o$-O surface oxide phase. We find that the prevalent structural model, a rumpled PdO(001) film suggested by previous low energy electron diffraction (LEED) work (M. Saidy *et al.*, Surf. Sci. **494**, L799 (2001)), is incompatible with all three employed methods. Instead, we suggest the two-dimensional film to consist of a strained PdO(101) layer on top of Pd(100). LEED intensity calculations show that this model is compatible with the experimental data of Saidy *et al.*

I. INTRODUCTION

Due to their importance for catalysis and corrosion, oxidation processes at transition metal (TM) surfaces have long received significant attention both in fundamental and applied research. Roughly divided into pure on-surface (dissociative) adsorption, surface-oxide formation, and oxide film growth, particularly the second step in the oxidation sequence is poorly understood on a microscopic level. Not least, this is due to the fact that an atomic-scale investigation of TM surfaces on the verge of oxide formation still poses a significant challenge for the otherwise well-developed machinery of ultra-high vacuum (UHV) surface science: The rather high oxygen partial pressures and elevated temperatures required to initiate oxide nucleation, a low degree of order at the surface and highly complex, large unit-cell geometries name but a few of the problems encountered on the route towards a microscopic characterization of surface oxides.

The vast structural parameter space connected with surface oxides is often prohibitive for an analysis based on one technique alone, in particular for the exhaustive searches required in diffraction-based structure determination techniques like low energy electron diffraction (LEED). Fortunately, over the last 10 years it became clear that the joint effort of experimental works and theory (in particular when using first-principles methods) is synergetic and most valueable, if not crucial, and allows a convincing identification and characterization of complex, novel structures at surfaces[1,2,3,4,5]. Such a multi-method approach is also adopted in the present work, where high-resolution core-level spectroscopy (HRCLS), scanning tunneling microscopy (STM), and density-functional theory (DFT) are employed addressing the Pd(100)-($\sqrt{5} \times \sqrt{5}$)$R27^o$-O surface oxide phase (coined $\sqrt{5}$-phase in the following for brevity), which for $T > 400\,\mathrm{K}$ concludes the series of ordered phases observed on Pd(100) before three-dimensional cluster growth sets in[6].

A previous tensor LEED analysis suggested the $\sqrt{5}$-phase to correspond essentially to a rumpled PdO(001) plane on top of Pd(100)[7,8]. In the following we will show that this assignment can not be reconciled with either HRCLS, STM, or DFT, the methods employed in the present study. Instead, we propose a new model, consisting of a strained PdO(101) layer on Pd(100). This is in agreement with all experimental data and energetically more stable than the previous model. Moreover, we performed preliminary LEED calculations to show that this new arrangement can also be reconciled with the previous experimental LEED data of Saidy *et al.*[8]. Interestingly, the (101) orientation does not correspond to a preferred growth direction[9] or a low-energy surface of crystalline PdO, suggesting that the film-substrate interaction may stabilize higher energy crystal faces. We argue that the atypical orientation and the resulting chemical properties of such thin oxide layers may be of interest in future applications.

II. EXPERIMENTAL AND COMPUTATIONAL DETAILS

The STM measurements were performed in a UHV chamber with a base pressure below $1 \times 10^{-10}\,\mathrm{mbar}$. The Pd(100) surface was cleaned by cycles of Ar^+ sputtering, annealing and oxygen treatments keeping the sample at $900\,\mathrm{K}$ in an oxygen pressure of $2 \times 10^{-8}\,\mathrm{mbar}$ followed by flashes to $1400\,\mathrm{K}$. The cleanliness of the Pd(100) surface was checked by Auger Electron Spectroscopy (AES); no contaminants such as C and O could be observed within the detection limits. The $\sqrt{5}$-phase was thereafter formed by exposing the Pd(100) surface to an oxygen pressure of $5 \times 10^{-6}\,\mathrm{mbar}$ for 300 seconds at $T = 600\,\mathrm{K}$.

The HRCLS measurements were conducted at the beam line I311[10]at MAXII in Lund, Sweden. The cleaning procedure and preparation of the $\sqrt{5}$-phase was identical to that described above. The HRCL spectra were

recorded at liquid nitrogen temperatures and at normal emission angle. The cleanliness of the Pd(100) surface was checked by monitoring the Pd $3d_{5/2}$, O $1s$, and C $1s$ core-levels, as well as the valence band region; again, no contaminants could be detected.

The DFT calculations were performed within the Full-Potential Linear Augmented Plane Wave (FP-LAPW) scheme[11,12,13] using the generalized gradient approximation (GGA)[14] for the exchange-correlation functional. The $\sqrt{5}$ surface oxide was modeled in a supercell geometry, employing a symmetric slab consisting of five layers Pd(100) in the middle plus the various PdO layers described below on both sides. A vacuum region of ≈ 15 Å ensures the decoupling of the surfaces of consecutive slabs. All atomic positions within the PdO and the outermost substrate layer were fully relaxed.

The FP-LAPW basis set parameters are as follows: $R_{\rm MT}^{\rm Pd}$ =1.8 bohr, $R_{\rm MT}^{\rm O}$ =1.3 bohr, wave function expansion inside the muffin tins up to $l_{\rm max}^{\rm wf} = 12$, potential expansion up to $l_{\rm max}^{\rm pot} = 4$, and a $(4 \times 4 \times 1)$ Monkhorst-Pack grid with 8 **k**-points in the irreducible part of the Brillouin zone (28 **k**-points in the full zone). The energy cutoff for the plane wave representation in the interstitial region between the muffin tin spheres was $E_{\rm wf}^{\rm max} = 20$ Ry for the wave functions and $E_{\rm pot}^{\rm max} = 169$ Ry for the potential. With this basis set very good agreement is obtained with the results of the structure determination for the $p(2 \times 2)$ phase on Pd(100) reported by a previous LEED study[15], and we find the relative energetic stabilities of the various tested overlayer models converged to within ± 50 meV per O atom.

This does, however, not comprise the uncertainty in the absolute binding energies, E_B. DFT, even within the GGA, is known to poorly describe gas phase oxygen and gives in particular the binding energy for molecular O_2 wrong by about 0.5 eV per O atom[16]. As this directly effects the obtained absolute binding energies for the various surface oxide phases, a possible workaround would be to determine the total energy of molecular oxygen, $E_{\rm O_2}^{\rm tot}$, not via gas phase calculations, but via[17]

$$1/2 E_{\rm O_2}^{\rm tot} \;\approx\; E_{\rm PdO,bulk}^{\rm tot} - E_{\rm Pd,bulk}^{\rm tot} + \Delta H_f(300{\rm K}, 1{\rm atm})$$

i.e. employing an approximate equation for the PdO heat of formation, ΔH_f, into which only the total energies of bulk PdO and Pd bulk, $E_{\rm PdO,bulk}^{\rm tot}$ and $E_{\rm Pd,bulk}^{\rm tot}$, enter. Using the experimental $\Delta H_f(300{\rm K}, 1{\rm atm})$ one can thus arrive at $E_{\rm O_2}^{\rm tot}$ without having to resort to atomic calculations, though at the expense of discarding a completely first-principles type description.

In the present work we will only compare the stability of various structural models all including the same number of oxygen atoms. Then, the difference between the standard computation of binding energies, i.e. utilizing gas-phase computed $E_{\rm O_2}^{\rm tot}$, and the aforedescribed procedure amounts only to a constant shift in the calculated binding energies. Employing $\Delta H_f^{\rm exp}(300{\rm K}, 1{\rm atm}) = 0.88$ eV[18], this shift amounts to 0.43 eV per O atom with a lower stability of the ΔH_f-derived binding energies and not including zero-point vibrations. This indicates the sizable uncertainty in the absolute binding energy values and correspondingly dictates a cautious judgement on the endo- or exothermicity of a structure. In the following, we will always indicate binding energies obtained with gas-phase computed $E_{\rm O_2}^{\rm tot}$ (not including zero-point vibrations), which according to the above argument are likely to represent an upper limit to the real stability. Our main conclusion, the rebuttal of the prevalent $\sqrt{5}$-model, will, however, rather be based on relative energetic differences, which are fortunately enough much better defined.

The surface core-level shift (SCLS), $\Delta_{\rm SCLS}$, is defined as the difference in energy which is needed to remove a core electron either from a surface or a bulk atom[19]. In the initial-state approximation the SCLS arises simply from the variation of the computed orbital eigenenergies before the excitation of the core electron. In final-state calculations, on the other hand, the SCLS involves an additional component due to the screening contribution from the valence electrons in response to the created core hole, obtained approximately via the Slater-Janak transition state approach of evaluating total energy differences using impurity type calculations as explained in detail in ref. 20. In case of the Pd $3d$ SCLSs the bulk level position can be employed as a well defined reference level to align theoretical and experimental spectra. For the O $1s$ levels however, we note that it is not very practical to also use the Pd $3d$ bulk-level position to align the O $1s$ data, as both types of orbital eigenenergies exhibit different convergence behavior with respect to the employed basis set. Also the Fermi-level position as another reference level present in both experimental and theoretical spectra is not very practical: Particularly for experiments on systems with high oxygen loads like surface oxides band bending can not be excluded.

Fortunately, we only need to rely on the existence (or non-existence) of a split O $1s$ spectrum in the present work. This difference in relative O $1s$ level positions of various atoms within the same geometry is well defined and independent of the reference zero used. Just in order to present the theoretical and experimental data in the same plot (Fig. 2) we will therefore employ the simplest possible alignment approach given by equating the position of the lowest theoretical and experimental O $1s$ core-level position. We stress that this crude procedure does not enter our physical argument and is solely used for graphical purposes.

III. RESULTS AND DISCUSSION

1. *Shortcomings of the prevalent $\sqrt{5}$-LEED model*

Fig. 1 shows the development of the experimental HRCL spectra from the O $1s$ and Pd $3d_{5/2}$ levels for the sequence of ordered structures that form on the Pd(100) surface with increasing oxygen coverage. After the two

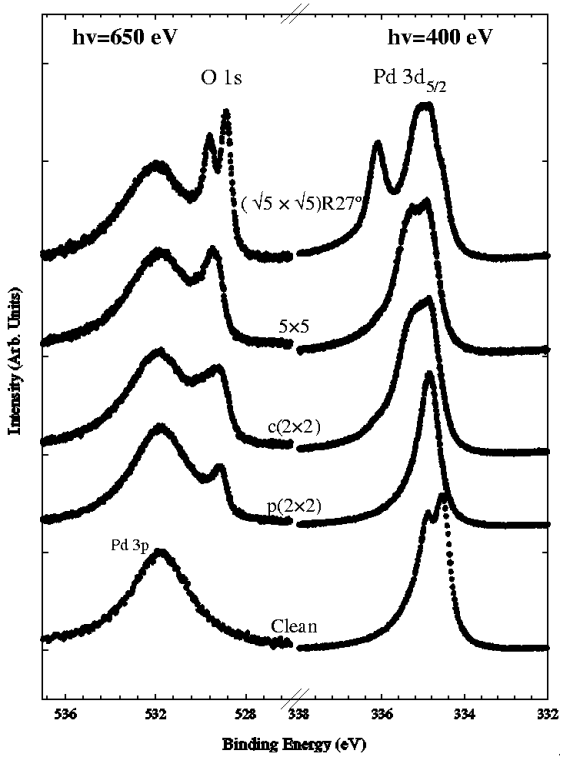

FIG. 1: Experimental HRCL spectra of the O 1s and the Pd $3d_{5/2}$ levels for the sequence of ordered structures that form on Pd(100) with increasing oxygen coverage. The photon energies were 650 eV and 400 eV respectively.

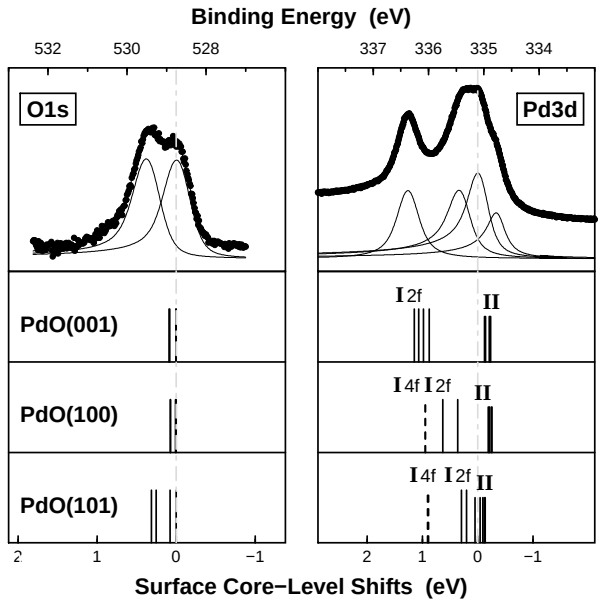

FIG. 2: Top panel: measured HRCL spectra of the O 1s and the Pd $3d_{5/2}$ levels from the Pd(100)-$(\sqrt{5}\times\sqrt{5})R27^o$-O phase at higher photon energies (900 eV and 650 eV for O 1s and Pd 3d, respectively) and with the Pd 3p contribution of the clean surface removed. Bottom panel: Calculated final-state shifts for the three structural models shown in Fig. 3. For Pd 3d the bulk-level is employed to align theoretical and experimental spectra. For O 1s the lowest-energy theoretical peak is simply aligned to the lowest-energy experimental peak (see text). Note that only the PdO(101) layer on Pd(100) exhibits a split O 1s spectrum with two significantly shifted components. See Fig. 3 for the nomenclature used to describe the atoms from which the various theoretical Pd core-level shifts originate.

known adsorption phases, $p(2\times2)$ at $\theta = 0.25$ ML and $c(2\times2)$ at $\theta = 0.50$ ML[15,21,22,23,24], at first an intermediate (5×5) surface oxide forms, before finally the $\sqrt{5}$ is obtained, on which we concentrate in this work. Focusing first on the O 1s spectrum of this $\sqrt{5}$-phase, its most surprising feature is the existence of two sharp peaks in contrast to the single peak observed at all lower coverage structures. As is apparent from Fig. 1, a definite assignment of these peaks is hampered by the energetically very close lying Pd 3p levels. Still, we attribute these two peaks to emission from O 1s levels as no similar features are observed at the low binding-energy side of the Pd 3d spectrum. Changing the incident photon energy to vary the escape depth of the photoelectrons leads us to conclude that they originate from oxygen atoms close to the surface and at roughly the same depth.

To arrive at a rough estimate of the relative coverages, we approximately remove the contribution from the Pd 3p levels by subtracting the Pd 3p spectrum recorded from the clean surface. The corresponding HRCL spectra for the $\sqrt{5}$-phase are shown in Fig. 2, now recorded at higher photon energies of 900 eV and 650 eV for the O 1s and Pd 3d levels, respectively. At the expense of a decreased resolution, these somewhat high energies are employed to avoid diffraction effects and thus permit a rough estimate of the relative coverages giving rise to the two peaks. We note that despite the decreased resolution, the two peaks are still clearly distinguishable in the original (not shown) and subtracted (Fig. 2) data. In both cases we obtain a considerable binding energy shift of ≈ 0.75 eV between both peaks and a ratio of about 1:1 for the two components. On the basis of this analysis of the experimental O 1s spectrum we would therefore anticipate at least two oxygen species at or close to the surface of the $\sqrt{5}$-phase in close to equal amounts.

Turning to the Pd $3d_{5/2}$ spectra in Fig. 2, at least three oxygen-induced components are experimentally resolved, at -0.32 eV, +0.38 eV and +1.30 eV, where a positive SCLS indicates a higher binding energy with respect to the reference Pd bulk component. Using simple initial-state arguments, we expect an increased oxygen coordination to yield a positive SCLS for the Pd $3d_{5/2}$ level. Thus, the component shifted by +1.30 eV could be due to highly oxygen coordinated Pd atoms, agreeing with previous results from the intermediate oxide structure on Pd(111)[5], in which a very similarly shifted component was found and assigned to Pd atoms fourfold coordinated to oxygen. The component shifted by +0.38 eV could correspondingly be due to Pd atoms coordinated

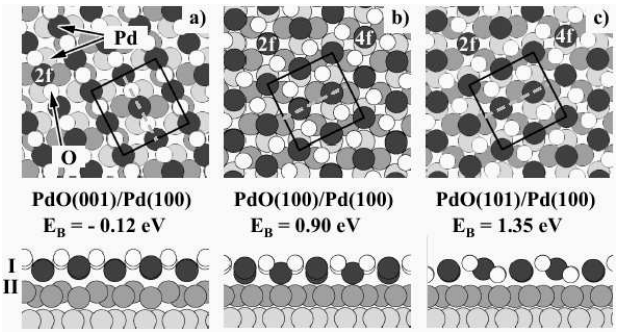

FIG. 3: Top- and side-view of the three structural models of the Pd(100)-$(\sqrt{5}\times\sqrt{5})R27^o$-O phase considered in the present work. All models assume an oxygen coverage of 0.8 ML. a) PdO(001) layer on Pd(100)[7,8], b) PdO(100) layer on Pd(100), and c) PdO(101) layer on Pd(100). The $\sqrt{5}$ unit-cell is sketched in the top-views (solid line), while the dashed lines indicate the direction of atomic rows seen in the STM images. The DFT binding energy of the three models clearly reveals the PdO(101) layer on Pd(100) as the most favorable model. $2f$ and $4f$ denote two- and fourfold coordinated first-layer Pd atoms, and relate to the labels in Fig. 2 used to specify the atomic origin of the various computed core-level shifts.

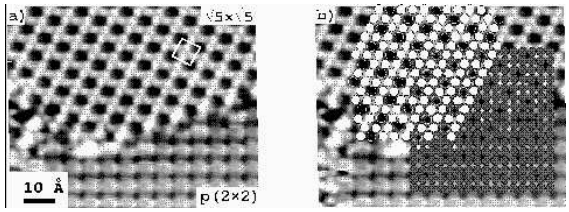

FIG. 4: a) STM image showing a domain boundary between the Pd(100)-$(\sqrt{5}\times\sqrt{5})R27^o$-O and the $p(2\times2)$ phase. b) The same STM image but with a Pd(100) lattice superimposed (grey circles). This shows directly that in the $\sqrt{5}$-phase bright spots (assigned to Pd atoms, white circles) are shifted in neighboring rows by half a nearest neighbor distance, and that the dark spots (Pd atoms in hollow sites, transparent circles) coincide with hollow sites of the underlying Pd(100) substrate (Tunnel parameters: V=0.76 V, I=0.57 nA).

to less oxygen atoms (possibly two or three), whereas the component shifted by -0.32 eV likely originates from Pd atoms at the interface between the Pd(100) substrate and the thin oxidic film.

Trying to analyze the compatibility of the present HRCLS data with the prevalent structural model of the $\sqrt{5}$-phase suggested on the basis of the tensor LEED analysis (henceforth abreviated with "LEED model")[7,8], cf. Fig. 3a, we used the published atomic positions of the LEED model as input to our DFT computations. Obtaining SCLS that did not resemble the experimental data at all, we initially proceeded by subjecting the LEED model to a complete structural relaxation. The resulting final-state SCLS after relaxation are shown in Fig. 2 and are still difficult to reconcile with the experimental data: The large splitting of the O $1s$ spectrum is not reproduced and almost identical O $1s$ positions are obtained for all O atoms in the structure. Recalling that the LEED model essentially corresponds to a PdO(001) overlayer on Pd(100), in which all oxygen atoms are in principle equivalent, cf. Fig. 3a, this result is not surprising. The agreement in case of the Pd $3d$ SCLSs is not much better, obtaining computed shifts that are split into two distinct groups in contrast to the four component structure seen experimentally.

Geometrically, the structural relaxation in DFT almost completely removes most of the strong rumpling introduced in the LEED study to fit the experimental $I(E)$-curves, and the substrate/oxide interface smoothes out at a large interface distance indicating a very weak coupling. In the end, the absolute binding energy per O atom, E_B, of the LEED model was (with the caveat given in Section II) still found to be slightly endothermic with respect to molecular oxygen ($E_B = -0.12$ eV/ O atom), adding to our doubts of this prevalent structural model of the $\sqrt{5}$-phase.

Finally, we also performed STM measurements of the $\sqrt{5}$-phase, a corresponding image of which is shown in Fig. 3a. As may directly be seen from the image, neighboring bright rows are shifted by half a nearest neighbor distance with respect to each other, in contrast to what would be expected from the PdO(001) geometry depicted in Fig. 3a. This finding (STM) together with the absence of a split in the calculated O $1s$ spectrum (HRCLS) and the low energetic stability (DFT) led us to conclude that the prevalent LEED $\sqrt{5}$-model is incompatible with the three methods employed in the present study.

2. Searching for a new model

To identify an alternative geometry of the $\sqrt{5}$-phase, we first further analyze our experimental STM data in order to reduce the vast phase space of possible structural models. The bottom right half of the STM image shown in Fig. 4a exhibits a domain of the coexisting $p(2\times2)$ on-surface adsorption phase, in which the oxygen overlayer simply occupies fourfold hollow sites of the underlying Pd(100) substrate[15,21,22,23,24]. Based on this known geometry and the frequent finding that oxygen would appear as dark spots in the STM image, we construct the Pd(100) lattice and superimpose it on the experimental image, as shown in Fig. 4b. It then follows that the dark spots in the $\sqrt{5}$-phase are directly situated on top of the fourfold hollow sites of the Pd(100) lattice.

Assuming that the bright protrusions in the STM image correspond to the geometric position of Pd atoms, we may further draw the Pd sublattice of the suspected surface oxide layer into the STM image as done in Fig. 4b. This way, a total of three Pd atoms per $\sqrt{5}$ unit-cell are found, forming a rather open interlaced ring-like layer, the structure of which doesn't resemble a bulk-like PdO planar nearest-neighbor environment at all. The latter

would instead be obtained, if Pd atoms would also be present at the position of the large dark spots, yielding then a more compact layer with a total of four Pd atoms per $\sqrt{5}$ unit-cell. As the dark spots are directly situated on top of the hollow substrate sites, a straightforward explanation why these latter Pd atoms do not show up in the STM images would e.g. be a large corrugation within the surface oxide overlayer, in which all Pd atoms over Pd(100) hollow sites are strongly relaxed inwards.

While we may thus tentatively determine the positions of the Pd atoms on the basis of the STM images, the latter do not lead to any conclusions about the position and number of oxygen atoms in the $\sqrt{5}$ unit-cell. Concerning the O coverage, we can however resort to the HRCLS measurements. Calibrating the spectra, cf. Fig. 1, with the $p(2 \times 2)$ (0.25 ML) and $c(2 \times 2)$ (0.50 ML) adsorbate structures known from the previous LEED work[15,21,22,23,24], a rough estimate of $\theta \sim 0.8$ ML is obtained, which would correspond to four O atoms per $\sqrt{5}$ unit-cell.

Using these experimental observations, we proceed to set up structural models that are compatible with the data discussed so far. Assuming the $\sqrt{5}$-phase to be some form of surface oxide on Pd(100), PdO-like overlayers seem a most appealing choice for a model. A systematic look at all possible low-index PdO planes turns up two orientations which exhibit Pd positions whose lateral arrangement would agree with that deduced from STM: PdO(100) and PdO(101), cf. Fig. 3b and 3c respectively. In contrast, the earlier LEED model consists essentially of a PdO(001) plane on Pd(100), which is *not* equivalent to PdO(100) due to the tetragonal unit-cell of PdO[25]. Hence, the LEED model features an orientation, which does not fit the STM data, as seen when comparing Fig. 3a with Fig. 4.

3. *PdO(101)/Pd(100) as the new model*

Having filtered out PdO(100) and PdO(101) as two possible candidates for a new structural model, we note that the two differ only in the vertical position of the oxygen atoms. Each structure contains four oxygen and four Pd atoms per $\sqrt{5}$ unit-cell, which nicely fits the experimental coverage estimate described in Section III.2 . Yet, PdO(100) has all four O atoms above the Pd layer, while PdO(101) has two up and two down, as can be seen in Figs. 3b and 3c respectively. To discern between the two orientations, we subjected both to a full structure optimization in our DFT calculations. Interestingly, this yields a significantly increased stability for both overlayer models: in both cases, the binding energy is more than 1 eV per O atom higher than that of the previous LEED model, thus providing the final evidence for the incorrectness of the latter. More precisely, we find the PdO(101)/Pd(100) $\sqrt{5}$-geometry to be the most stable of the three structural models depicted in Fig. 3 with a binding energy of $E_B = +1.35$ eV / O atom (compared to

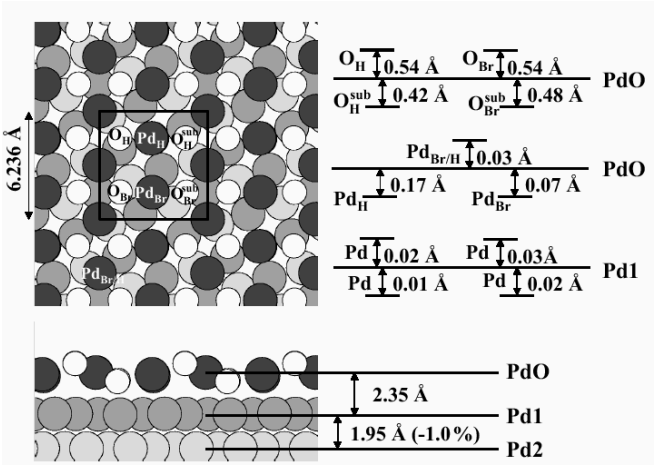

FIG. 5: Top- and side-view of the PdO(101)/Pd(100) model for the $\sqrt{5}$-phase on the basis of the DFT calculations. The rumpling of both the O and Pd atoms in the PdO overlayer and of the Pd atoms in the topmost substrate layer is given with respect to the center of mass of the respective layers. In the bottom right, also the average layer distances between these center of mass are indicated.

$E_B = -0.12$ eV / O atom for the LEED model and $E_B = +0.90$ eV / O atom for the PdO(100) overlayer).

Further checking on PdO(101)/Pd(100) as our new structural model, we also calculated a number of geometries keeping the positions of the Pd atoms in the overlayer, but testing different lateral positions for the O atoms. In particular, this involved geometries, where some oxygen atoms were located in bridge sites between the overlayer Pd atoms to produce differently coordinated O atoms at the surface that could then possibly also generate a split O 1*s* core-level spectrum. Yet, in all such combinatorial cases with O in hollow and bridge sites we obtained binding energies more than 0.2 eV lower than for our PdO(101)/Pd(100) model. As second test series, we tried different registries of the PdO(101) overlayer on Pd(100), i.e. we laterally shifted the PdO overlayer around on the substrate. Again, this always resulted in a lower stability with respect to the structure shown in Fig. 3c. Finally, the dark holes seen in the STM image suggested that one of the four overlayer Pd atoms could be absent, namely the one over the fourfold hollow site, Pd_H in Fig. 5. With bulk Pd as reservoir for the removed Pd atom, we also find such a model to be less stable. In conclusion, the DFT calculations therefore strongly favor the PdO(101)/Pd(100) structure for the $\sqrt{5}$-phase.

To see whether this new model is also compatible with the presented experimental HRCLS data, we show its computed final-state SCLS in Fig. 2 and list all its Pd 3*d* shifts in Table I. Comparing with the shifts obtained for the LEED model and for PdO(100)/Pd(100), cf. Figs. 3a and 3b, PdO(101) is the only model that exhibits an appreciably split O1*s* core-level spectrum, due to the presence of both on- and sub-surface O in the geome-

	Initial	Screening	Final	Experiment
I_{4f}, $Pd_{Br/H}$	+0.79	+0.10	+0.89	+1.30
	+0.86	+0.05	+0.91	
I_{2f}, Pd_{Br}	+0.20	+0.09	+0.29	+0.38
Pd_{H}	+0.18	+0.21	+0.39	
II, Pd1	-0.31	+0.18	-0.13	
	-0.28	+0.19	-0.09	
	-0.26	+0.15	-0.11	-0.32
	+0.01	-0.05	-0.04	
	+0.16	-0.11	+0.05	

TABLE I: Calculated and measured Pd 3*d* surface core-level shifts for the PdO(101)/Pd(100) model in eV. The computed values are separated into initial-state and screening contribution, yielding the total final-state shift that can be compared to experiment. See Figs. 2 and 5 for the notation to describe the various first (I) and second (II) layer atoms.

try, cf. Fig. 2. The obtained Pd 3*d* shifts of +0.9 eV and +0.4 eV due to fourfold and twofold oxygen coordinated Pd atoms in the PdO(101) overlayer, $Pd_{Br/H}$ and Pd_{Br}/Pd_{H} in Fig. 5, compare reasonably with the two experimental peaks that had already been assigned to differently coordinated Pd atoms on the basis of initial-state arguments. The remaining experimentally resolved peak with a small negative shift had similarly been attributed to the top Pd substrate atoms at the interface, which in the calculations exhibit almost vanishing SCLSs (Pd1 in Fig. 5).

Of course, the very structure of the PdO(101) overlayer with an equal amount of on- and sub-surface oxygen atoms renders the measured splitted O 1*s* spectrum immediately plausible. In fact, the significant rumpling together with the different sub-surface O coordination to the underlying substrate, cf. Fig. 5, yield even slightly different shifts for the two atoms of each oxygen species present in the $\sqrt{5}$ unit-cell, cf. Fig. 2. Averaging the contributions within each group, we obtain a computed initial (final) state shift of 0.55 eV (0.49 eV) between the O 1*s* peaks due to on- and sub-surface oxygen atoms, in reasonable agreement with the measured value of 0.75 eV.

4. Compatibility with existing LEED data

So far, we have shown that our new model is superior to the model of Saidy *et al.*[7,8] with respect to all three techniques employed in the present work (HRCLS, STM, DFT). On the other hand, the model of Saidy *et al.* has strong backing from quantitative LEED. Hence, a final verification of our model would be to establish its viability also by this method. To accomplish this goal, we performed a rather restricted set of LEED $I(E)$ calculations for our structural model, comparing them to the very set of experimental LEED data published by Saidy *et al.*[8] (scanned and digitized from their Fig. 2). From this we may judge whether or not our geometry can yield LEED $I(E)$ spectra on par or superior to those of Saidy *et al.* Our quantitative LEED calculations utilized the TensErLEED program package[26], employing 10 fully relativistic phase shifts and a first-principles, energy-dependent real part of the inner potential, both generated for the surface geometry of Fig. 5 using Rundgren's phase shift program package[27]. Where the Tensor LEED method[28,29] was employed, care was taken to ensure the full-dynamic reproducibility of the results in the final step of the calculation. All non-structural parameters of the calculation were kept fixed at the values chosen by Saidy *et al.*

As a first step, we simply used the exact optimized geometry of the DFT-GGA calculations as input to the full-dynamic part of the TensErLEED code. Already this produced $I(E)$ curves in reassuring visual agreement with the scanned experimental spectra – i.e., all major spectral features could be reproduced. Still, shifts between individual peaks and overall shape difference only allowed for an average Pendry R-factor[30] $R_{\mathrm{P}} = 0.51$ between calculated and scanned $I(E)$. Hence, in a second step, we used the Tensor LEED method to relax all vertical positions in the PdO(101) layer, as well as the topmost two Pd(100) substrate layers below. The result of this is a clear drop of the best-fit Pendry R-factor to $R_{\mathrm{P}} = 0.28$, shared by both integer ($R_{\mathrm{int}} = 0.29$) and fractional ($R_{\mathrm{frac}} = 0.28$) beams on average. The improvement is mainly due to overall slightly expanded distances between the individual layers compared to the DFT-GGA result. Moreover, a significant buckling is found in the second substrate layer, which was not relaxed in DFT. Of course, some differences of this kind must be expected already because no lateral or non-structural degrees of freedom were adjusted in the LEED fit. While the latter parameters may well account also for the remaining discrepancies between calculated and experimental $I(E)$ curves, the main goal of our LEED calculations has clearly been achieved: Already a very limited structural refinement of PdO(101)/Pd(100) produces experiment-theory agreement at a level which is even slightly improved compared to that presented by Saidy *et al.* ($R_{\mathrm{P}} = 0.306$)[8] in their analysis. The consistency of our model with all available experimental data is thus established.

5. Strained PdO(101)/Pd(100)

The new structural model for the $\sqrt{5}$-phase is essentially a strained and rumpled PdO(101) film on top of Pd(100). The PdO(101) in-plane lattice constant is almost equal to that of a $\sqrt{5}$ unit-cell on Pd(100), with the unit surface area of the commensurable film found here smaller by only 1.4% than for unstrained PdO(101). On the other hand, we compute a rather strong coupling of 100 meV/Å^2 of the laterally compressed PdO over-

layer to the underlying Pd(100) substrate, rationalizing the formation of a commensurable surface oxide structure. This strong coupling also helps to stabilize the particular PdO(101) orientation, which is experimentally not found to be a preferred growth direction of PdO crystallites[9]. Our calculations show that the stoichiometric termination of bulk PdO(101)-(1×1) suggested in the $\sqrt{5}$-film, i.e. the one terminated by O atoms as shown in Fig. 5, is in fact considerably more stable than the two other ways of truncating PdO in (101) direction, 57 meV/Å^2 compared to 134 meV/Å^2 (also O terminated) and 128 meV/Å^2 (Pd terminated)[31]. Interestingly, the bulk PdO(100) orientation shown in Fig. 3b exhibits even a significantly lower surface energy (33 meV/Å^2), while this orientation is in the commensurable thin film geometry discussed here energetically not as favorable as the PdO(101) $\sqrt{5}$-model. Evidently, the presence of oxygen at the oxide/metal interface yields a stronger coupling to the underlying substrate and is ultimately responsible for the higher stability of the PdO(101)/Pd(100) surface oxide geometry.

This example of the stabilisation of a higher energy crystal face in thin oxide films due to strong interfacial coupling to the substrate adds another interesting aspect to the new physics found recently in studies concerning oxide formation at TM surfaces. Among other findings, the formation of incommensurable domains of low energy oxide faces has been reported for ruthenium single crystals[32,33], delineating the opposite case to the results reported here, i.e. when the oxide orientation is more important than a good coupling to the underlying substrate. Apparently, the lower thermal stability of palladium oxides compared to RuO_2 increases the importance of the oxide/metal interface. This is further supported by the surface oxide structure just found on Pd(111), which does not resemble any PdO bulk orientation at all[5].

Experimentally, oxide thicknesses below about 20 Å have been found in all of these cases, indicating either a slow growth kinetics once the thin films have formed or a thermodynamic hindrance to form thick bulk oxides. This could be of interest in oxidation catalysis, where such oxide patches forming on TM surfaces in the reactive environment are now discussed as the actually active material[32,34,35,36]. If a continued growth of these oxide films is not possible, so that their structure always remains significantly affected by the interfacial coupling, they may exhibit catalytic behavior which is non-scalable from corresponding bulk oxide crystallites - in other words, truly nano-catalytic properties. Even when the oxide growth is not limited, the structure of the initially formed oxide film will be crucial, setting the stage for the ensuing oxidation process. For thicker films, interfacial coupling will be progressively less influential, so that an initially stabilized higher energy oxide orientation as found in the present work should eventually become liable to faceting. The corresponding three-dimensional cluster growth has indeed been observed for the continued oxidation of both Pd(100) and Pd(111)[6,37].

IV. SUMMARY

In conclusion, we have shown that the prevalent structural model for the Pd(100)-$(\sqrt{5}\times\sqrt{5})R27^o$-O surface oxide can not be reconciled with neither the experimental nor the theoretical methods employed in the present study: Its surface symmetry does not fit to the one observed by STM, and the calculated HRCLS for this structure do not show the appreciable splitting of the O 1s spectrum observed experimentally. In addition DFT calculations give only a very low energetic stability and a relaxed geometry that does no longer exhibit the significant rumpling originally introduced to match the measured LEED $I(E)$ curves.

Based on the present experimental data we reanalyze the $\sqrt{5}$-phase and suggest an alternative structural model: a strained PdO(101) layer on Pd(100). This arrangement is energetically much more stable in our DFT calculations. Its computed final-state SCLSs agree well with all HRCLS measurements, linking the large splitting of the O 1s spectrum to the presence of oxygen both at the surface and at the oxide/metal interface. Already a very restricted set of LEED intensity calculations establishes the compatibility of this structure also with the previously published LEED intensity data.

The PdO(101) orientation, which is experimentally not found to be a preferred PdO growth direction, is stabilized by the strong coupling to the underlying substrate in the present thin film limit. In comparison to the ensuing three-dimensional cluster growth during continued oxidation, the $\sqrt{5}$-phase is therefore likely to display different physico-chemical properties, which might be of interest or relevance to high-pressure applications like catalysis.

V. ACKNOWLEDGEMENTS

We are thankful for partial support by the DFG priority program "Realkatalyse". The support from the MAXLAB staff and financial support from the Swedish Research Council is gratefully acknowledged. Stimulating discussions with Georg Kresse are also gratefully acknowledged.

[1] A. Schmalz, S. Aminpirooz, L. Becker, J. Haase, J. Neugebauer, M. Scheffler, D.R. Batchelor, D.L. Adams, and E. Bøgh, Phys. Rev. Lett. **67**, 2163 (1991).

[2] J. Burchhardt, M.M. Nielsen, D.L. Adams, E. Lundgren,

J.N. Andersen, C. Stampfl, M. Scheffler, A. Schmalz, S. Aminpirooz, and J. Haase, Phys. Rev. Lett. **74**, 1617 (1995).
[3] C. Stampfl, S. Schwegmann, H. Over, M. Scheffler, and G. Ertl, Phys. Rev. Lett. **77**, 3371 (1996).
[4] S.-H. Lee, W. Moritz, and M. Scheffler, Phys. Rev. Lett. **85**, 3890 (2000).
[5] E. Lundgren, G. Kresse, C. Klein, M. Borg, J.N. Andersen, M. De Santis, Y. Gauthier, C. Konvicka, M. Schmid, and P. Varga, Phys. Rev. Lett. **88**, 246103 (2002).
[6] G. Zheng and E.I. Altman, Surf. Sci. **504**, 253 (2002).
[7] D.T. Vu, K.A.R. Mitchell, O.L. Warren, and P.A. Thiel, Surf. Sci. **318**, 129 (1994).
[8] M. Saidy, O.L. Warren, P.A. Thiel, and K.A.R. Mitchell, Surf. Sci. **494**, L799 (2001).
[9] J. McBride, K. Hass, and W. Weber, Phys. Rev. B **44**, 5016 (1991).
[10] R. Nyholm *et al.*, Nucl. Instr. and Meth. A **467**, 520 (2001).
[11] P. Blaha, K. Schwarz, and J. Luitz, **WIEN97**, *A Full Potential Linearized Augmented Plane Wave Package for Calculating Crystal Properties*, Karlheinz Schwarz, Techn. Universität Wien, Austria, (1999). ISBN 3-9501031-0-4.
[12] B. Kohler, S. Wilke, M. Scheffler, R. Kouba, and C. Ambrosch-Draxl, Comput. Phys. Commun. **94**, 31 (1996).
[13] M. Petersen, F. Wagner, L. Hufnagel, M. Scheffler, P. Blaha, and K. Schwarz, Comp. Phys. Commun. **126**, 294 (2000).
[14] J.P. Perdew, S. Burke, and M. Ernzerhof, Phys. Rev. Lett. **77**, 3865 (1996).
[15] D. Kolthoff, D. Jürgens, C. Schwennicke, and H. Pfnür, Surf. Sci. **365**, 374 (1996).
[16] M.V. Ganduglia-Pirovano and M. Scheffler, Phys. Rev. B **59**, 15533 (1999).
[17] W.X. Li, C. Stampfl, and M. Scheffler, Phys. Rev. B **67**, 045408 (2003).
[18] *CRC Handbook of Chemistry and Physics*, CRC press (Boca Raton, FL, 1995).
[19] D. Spanjaard, C. Guillot, M.C. Desjonqueres, G. Treglia, and J. Lecante, Surf. Sci. Rep. **5**, 1 (1985); W. F. Egelhoff, Surf. Sci. Rep. **6**, 253 (1987).
[20] S. Lizzit, A. Baraldi, A. Groso, K. Reuter, M.V. Ganduglia-Pirovano, C. Stampfl, M. Scheffler, M. Stichler, C. Keller, W. Wurth, and D. Menzel, Phys. Rev. B **63**, 205419 (2001).
[21] T.W. Orent and S.D. Bader, Surf. Sci. **115**, 323 (1982).
[22] E.M. Stuve, R.J. Madix, and C.R. Brundle, Surf. Sci. **146**, 155 (1984).
[23] S.-L. Chang and P.A. Thiel, J. Chem. Phys. **88**, 2071 (1988).
[24] S.-L. Chang, P.A. Thiel, and J.W. Evans, Surf. Sci. **205**, 117 (1988).
[25] D. Rogers, R. Shannon, and J. Gillson, J. Solid State Chem. **3**, 314 (1971).
[26] V. Blum and K. Heinz, Comp. Phys. Comm. **134**, 392 (2001).
[27] J. Rundgren, Phase shift package (private communication, 2001, and to be published).
[28] P.J. Rous, J.B. Pendry, D.K. Saldin, K. Heinz, K. Müller, and N. Bickel, Phys. Rev. Lett. **57**, 2951 (1986).
[29] P.J. Rous, Prog. Surf. Sci. **39**, 3 (1992).
[30] J.B. Pendry, J. Phys. C **13**, 937 (1980).
[31] J. Rogal, K. Reuter, and M. Scheffler, (to be published).
[32] H. Over, Y.D. Kim, A.P. Seitsonen, S. Wendt, E. Lundgren, M. Schmid, P. Varga, A. Morgante, and G. Ertl, Science **287**, 1474 (2000).
[33] Y.D. Kim, A.P. Seitsonen, and H. Over, J. Phys. Chem B **105**, 2205 (2001).
[34] B.L.M. Hendriksen and J.W.M. Frenken, Phys. Rev. Lett. **89**, 046101 (2002).
[35] C. Stampfl, M.V. Ganduglia-Pirovano, K. Reuter, and M. Scheffler, Surf. Sci. **500**, 368 (2002).
[36] K. Reuter and M. Scheffler, Phys. Rev. Lett. **90**, 046103 (2003).
[37] G. Zheng and E.I. Altman, Surf. Sci. **462**, 151 (2000).